

Graphene on hexagonal boron nitride as an agile hyperbolic metamaterial

S. Dai¹, Q. Ma², S. -E. Zhu³, M. K. Liu^{1,4}, T. Andersen², Z. Fei¹, M. Goldflam¹, M. Wagner¹, K. Watanabe⁵, T. Taniguchi⁵, M. Thiemens⁶, F. Keilmann⁷, G. C. A. M. Janssen³, P. Jarillo-Herrero², M. M. Fogler¹, D. N. Basov^{1*}.

¹*Department of Physics, University of California, San Diego, La Jolla, California 92093, USA*

²*Department of Physics, Massachusetts Institute of Technology, Cambridge, Massachusetts 02215, USA*

³*Micro and Nano Engineering Lab, Department of Precision and Microsystems Engineering, TU Delft, Mekelweg 2, 2628 CD Delft, The Netherlands*

⁴*Department of Physics, Stony Brook University, Stony Brook, New York 11794, USA*

⁵*National Institute for Materials Science, Namiki 1-1, Tsukuba, Ibaraki 305-0044, Japan*

⁶*Department of Chemistry and Biochemistry, University of California, San Diego, La Jolla, California 92093, USA*

⁷*Ludwig-Maximilians-Universität and Center for Nanoscience, 80539 München, Germany*

*Correspondence to: dbasov@physics.ucsd.edu

Abstract

We have implemented and investigated the tunable hyperbolic response in heterostructures comprised of a monolayer graphene deposited on hexagonal boron nitride (G-hBN) slabs. Electrostatic gating of the graphene layer enables electronic tunability of phonon polaritonic properties of hBN: a layered material with well-documented hyperbolic response in the mid-infrared (mid-IR) frequencies. The tunability originates from the hybridization of surface plasmon polaritons in graphene to hyperbolic phonon polaritons in hBN: an effect that we examined via nano-IR imaging and spectroscopy. The hybrid polaritons possess combined virtues from plasmons in graphene and phonon polaritons in hBN. Therefore, G-hBN structures fulfill the definition of the electromagnetic metamaterial since the attained property of these devices is not revealed by its constituent elements. Our results uncover a practical approach for realization of agile nano-photonic metamaterials by exploiting the interaction of distinct types of polaritonic modes hosted by different constituent layers of van der Waals heterostructures.

Van der Waals (vdW) heterostructures assembled from (one or few) monolayers of graphene, hBN, MoS₂ and other atomic crystals in various combinations are emerging as a new paradigm to attain the desired electronic^{1,2} and optical^{3,4} properties. These heterostructures are also of interest in the context of effects derived from polaritons: collective modes originating from the coupling between optical photons and electric dipoles that are ubiquitous in metals, insulators and semiconductors⁵. At least two different classes of propagating polaritons are firmly established in vdW systems: surface plasmon polaritons (SPP or SP²) in graphene⁶⁻¹¹ and hyperbolic phonon polaritons (HPP or HP²) in hBN¹²⁻¹⁶. The qualifier “hyperbolic” pertains to a peculiar form of the electromagnetic response in highly anisotropic media when the axial and tangential components of the dielectric tensor (ϵ^z and $\epsilon^t \equiv \epsilon^x = \epsilon^y$) reveal the opposite signs^{17,18}. In essence, the HP²s are the extraordinary rays of anomalously high momenta. In hBN, the negative signs of ϵ^t and ϵ^z necessary for hyperbolic response arise due to, respectively, in- and out-of-plane optical phonons^{12,13}. Finite-thickness slabs of hBN act as multi-mode waveguides for HP²s. The modal wavelengths have been shown to scale linearly with the thickness of the hBN slabs¹². However, continuous and reversible control of these modes seems challenging because the electrodynamics of HP² is ultimately governed by a material’s crystal lattice. In contrast, SP² can be readily controlled electrically by varying the graphene Fermi energy⁶⁻¹¹. Demonstrating a similar reversible tunability of phonon polariton characteristics will be extremely interesting from the point of view of fundamental physics and also very desirable for applications¹⁷⁻²².

In this work, we report on a tunable hyperbolic response in vdW heterostructures that consists of graphene and hBN (G-hBN) as the two constituent elements. The tunable

properties of this G-hBN structure stem from electromagnetic coupling of plasmons and phonons²³⁻²⁴. The eigenmodes of the G-hBN structures are therefore plasmon-phonon polaritons produced by coherent oscillations of the electron density in graphene and the atomic vibrations in hBN. Surface plasmon-phonon modes²⁵ and related energy transfer processes²⁶ have been investigated in structures comprised of graphene with monolayer hBN or a BN nanotube. However, neither monolayers²⁵ nor nanotubes²⁶ of BN support hyperbolic response: an attribute of three-dimensional specimens of this layered anisotropic material^{12,13,16-18}. A remarkable feature of G-hBN heterostructures uncovered in our experiments is that monolayer graphene impacts the hyperbolic response of hBN slabs as thick as 99 nm, exceeding 300 atomic layers. We demonstrate by direct nano-IR imaging that both the wavelength and intensity of hyperbolic polaritons in these vdW devices can be controlled via electrostatic gating of the top graphene layer. Since such a tunable hyperbolic response is an attribute of the multilayer structure rather than its constituent elements, G-hBN can be classified as an electromagnetic metamaterial²⁷.

Direct experimental access to tunable hyperbolic response in G-hBN is provided by IR nano-spectroscopy and nano-imaging via a scattering-type scanning near-field optical microscope (s-SNOM) as shown in Fig. 1a (see also Methods). The same technique has been utilized in a recent study²⁸ of hBN-G-hBN vdW heterostructures; however, the hyperbolic spectral regions were not probed therein. In Fig. 1b we show broad-band nano-IR spectra of the normalized (Methods) scattering amplitude $s(\omega)$ as a function of frequency $\omega = 1 / \lambda_{\text{IR}}$, λ_{IR} being the IR wavelength, for hBN, SiO₂ substrate, and G-hBN meta-structures. The spectra for SiO₂ (black) and hBN (red) display resonances due to their mid-IR phonons^{12,29}. The two hyperbolic regions of hBN^{12,13} are highlighted in

Fig. 1b. Type I region where $\varepsilon^z < 0$, $\varepsilon^t > 0$ extends over the frequency range $\omega = 746 - 819 \text{ cm}^{-1}$. Type II region where $\varepsilon^z > 0$, $\varepsilon^t < 0$ spans the range $\omega = 1370 - 1610 \text{ cm}^{-1}$. Both type I and type II resonances of hBN are modified in meta-structures incorporating a monolayer graphene (the blue spectrum in Fig. 1b). The impact of graphene is particularly prominent in the type I region where the resonance mode is significantly enhanced and blue-shifted by nearly $\sim 25 \text{ cm}^{-1}$ compared to the response of a standalone hBN slab.

The peculiar electrodynamics of G-hBN is vividly illustrated by the calculated frequency (ω) – momentum (q) dispersion relations of its polariton modes (Figs. 1c-e, see Supplementary Section 1 for details). Following Ref. 5, we visualize these dispersions using a false color map of the imaginary part of the reflectivity r_p . It is instructive to first consider the polaritons of the two constituent elements (graphene and hBN) separately. In Fig. 1c we plot the dispersion of SP^2 for a free-standing graphene layer for three selected values of the Fermi energy E_F . These parabolic curves are described by the equation³⁰

$q_p(\omega) = \frac{(\hbar\omega)^2}{2e^2 E_F}$. The corresponding plasmon wavelength is

$$\lambda_p = \frac{2\pi}{q_p} = 119 \text{ cm} \frac{E_F(\text{eV})}{[\omega(\text{cm}^{-1})]^2}. \quad (1)$$

Next, in Fig. 1d we plot the dispersion of HP^2 s in an hBN slab of thickness $d = 58 \text{ nm}$ on a SiO_2 substrate (no graphene). In a stark contrast to isotropic crystals where longitudinal optical phonons occur at a single degenerate frequency ω_{LO} , in hBN multiple distinct branches of HP^2 exist^{12,13}. These different branches correspond to quantized HP^2 waveguide modes with a scalar potential oscillating across the slab thickness and having different number of nodes. Each waveguide mode disperses between the two limits, ω_{TO}

and ω_{LO} (Fig. 1b). Our theoretical results and discussion below are relevant for all these modes; however, the experimental results concern exclusively the principal one, the nodeless waveguide mode of the lowest momentum. Finally, in Fig. 1e we display the dispersion of the new collective modes – hyperbolic plasmon-phonon polaritons (HP³) – that arise from mixing of the plasmons and hyperbolic phonon polaritons in the complete G-hBN meta-structure. The graphene Fermi energy $E_F = 0.37$ eV was estimated from the surface polariton wavelength in Fig. 3d (see also Ref. 28). The modification of hyperbolic response is clearly manifested in the blueshift of the HP³ frequencies with respect to those of HP² (Figs. 1d,e). The shift of momenta (at a fixed frequency) is opposite in the two hyperbolic bands: negative in the upper, type II band and positive in the lower, type I band. This contrasting behavior stems from the slopes of the dispersion curves being of opposite sign in the type I and II regions. Note that these slopes define the group velocities of the modes.

The change of the polariton wavelength induced by graphene is described by the formula:

$$\Delta\lambda(\%) = \frac{\lambda_{\text{HP}^3} - \lambda_{\text{HP}^2}}{\lambda_{\text{HP}^2}} \simeq \frac{\lambda_p}{\pi d} \frac{\varepsilon^z}{1 - \varepsilon^z \varepsilon^t} \quad (2)$$

Derivation of Eq. 2 and domain of its validity ($\frac{\lambda_{\text{HP}^2}}{\lambda_p} \gg \min \{2, |\varepsilon^z \varepsilon^t|^{-1/2}\}$) are discussed in the Supplementary Section 1. In a typical situation where $\varepsilon^z, \varepsilon^t$ are neither too large nor too small, this formula predicts that $\Delta\lambda(\%)$ is of the order of the ratio of the two length scales: the plasmon wavelength λ_p of graphene and the thickness d of hBN. This is consistent with physical expectations that the length scale over which graphene can exert its influence on the electrodynamics of surrounding media is set by its plasmon

wavelength. The latter can be controlled with the gate voltage. Thus, HP^3 s inherit the hyperbolic nature of HP^2 while gaining an important added virtue: tunability with the applied gate voltage. Outside the two HP^3 regions, the dispersion largely preserves the plasmonic character, see Fig. 1e. The latter mode flattens out in the vicinity of ω_{TO} phonon frequencies of either of the two hyperbolic bands: a consequence of the mode repulsion phenomenon. Similar interaction between plasmons and phonons has been studied in graphene on other substrates (e.g., SiO_2 , SiC , ion gel et al.) and monolayer hBN^{6-11,25,29}, where the hyperbolic response is not supported. Following the terminology established therein, we refer to the collective modes existing outside the hBN hyperbolic bands as the surface plasmon-phonon polaritons (SP^3)^{25,28}.

We now proceed with the analysis of IR nano-imaging data that visualize the propagating polaritons in our meta-structures and unambiguously support the above theoretical predictions. The basic principles of nano-IR imaging of polaritons have been detailed elsewhere^{7,8,12}. In short, when illuminated by the IR beam, the s-SNOM tip launches radially propagating polariton waves (Fig. 1a). The tip then registers the interference pattern between launched and edge-reflected polaritons, yielding oscillating fringes in the scattered near-field signal. The periodicity of the fringes is one-half of the polariton wavelength (denoted generically by λ , with suitable subscripts when needed).

In Fig. 2a we present IR nano-imaging data at a representative frequency $\omega = 1495 \text{ cm}^{-1}$ for a meta-structure that includes a slab of hBN of thickness $d = 25 \text{ nm}$ partially covered by a heavily doped monolayer graphene. We observe polariton fringes in both covered (G-hBN) and uncovered (hBN) parts. In the hBN region (the bottom half of Fig. 2a), the fringes originate from the type II hyperbolic polaritons¹². In the G-hBN

region (the upper part of the image in the middle of Fig. 2a) we observe fringes that are stronger and have a longer oscillation period. Prominent fringes can also be detected along the graphene edge (the dashed green lines). Line profiles obtained normal to the hBN edge (Fig. 2b) help to quantify the nearly 50% increase of both amplitude and wavelength of the fringe oscillations due to the presence of doped graphene. These modified fringes are assigned to plasmon-phonon coupling and the formation of the type II HP³ band in our meta-structure (Figs. 1e and 2c).

We observe similar enhancement of polaritonic oscillations (Figs. 2a-b) at all ω within the Type II band. Blue dots in Fig. 2c display these data in the form of the dispersion relation: ω plotted versus the polariton momentum q that can be read off the line profiles as $q = 2\pi / \lambda$. For comparison, we also obtained the HP² dispersion for pristine hBN (red triangles in Fig. 2c). Both data sets match the theoretical calculations (false color and white lines, see Supplementary Section 1 for details). The largest experimentally observed $\Delta\lambda(\%)=90\%$ in this data is reached at $\omega = 1545 \text{ cm}^{-1}$. In comparison, the approximate Eq. 2 yields 98%, using $d=25 \text{ nm}$, $\lambda_p=180 \text{ nm}$ (Eq. 1), $\epsilon^z=2.77$, and $\epsilon^t=-1.98$. The agreement between the experiment, analytical theory, and numerical simulations attests to the validity of the plasmon-phonon coupling approach to account for the modified spectrum of hyperbolic phonon polaritons. We performed measurements for a variety of samples, e.g., graphene on hBN of different thicknesses, graphene produced by exfoliation and chemical vapor deposition (CVD) techniques, all of which produced consistent results.

We now demonstrate the tuning of polaritons in the type II HP³ region via electrostatic gating. In this experiment, the gate voltage was applied between the Si

substrate and the top graphene layer (Methods). These results are shown in Figs. 3a-b at another representative frequency $\omega = 1395 \text{ cm}^{-1}$. When graphene is close to charge neutrality (Fig. 3a), the profile of propagating polariton in G-hBN is nearly indistinguishable from that of unobscured hBN. Once graphene is doped by gating (Fig. 3b), both the intensity and wavelength of the polaritonic features were significantly increased. This systematic study of the gate-tunability is summarized in Fig. 3c, where the wavelength (blue dots) consistently increases with the absolute value of gate voltage at fixed frequency $\omega = 1395 \text{ cm}^{-1}$.

We now wish to stress the distinction between the electrodynamics in HP³ and SP³ spectral regions (Fig. 1e). The latter are localized on the sample surface whereas the former propagate through the entire G-hBN meta-structure (Fig. 3d, inset) in the form of guided waves. We verified the waveguiding character by examining the thickness-dependence of HP³ wavelength using multiple hBN slabs covered by a large sheet of CVD graphene. The Fermi energy for all the G-hBN samples was about the same, $E_F = 0.37 \text{ eV}$. Both in experiment (blue dots) and simulations (green line), the dependence of the HP³ wavelength λ_{HP^3} on d is close to the linear law with a finite intercept (Fig. 3d and Supplementary Information). This law readily follows from two analytical results: $\Delta\lambda(\%) \sim d^{-1}$ (per Eq. 2) and $\lambda_{\text{HP}^2} \sim d$ (per Ref. 12). In contrast, the localized SP³ modes show essentially thickness-independent behavior of the polariton fringes outside the hyperbolic region (e.g., $\omega = 882 \text{ cm}^{-1}$).

Our work demonstrates that electronic, plasmonic and phonon polaritonic effects in layered vdW meta-structures are inherently intertwined. The strong optical anisotropy of the two-dimensional layered crystals that compose these structures is the key to

hyperbolic response, which creates propagating hybrid modes guided by the entire meta-structure slab, in addition to previously studied hybrid modes bound to the interfaces^{7-11,25}. The fundamental difference between HP^3 and SP^3 is illustrated by the polariton field simulations (yellow traces in Fig. 3d, inset). The field distribution of HP^3 in G-hBN is characteristic of a standing wave, whereas that of the SP^3 is localized at the G-hBN interface and exhibits an evanescent decay in the interior of the hBN crystal.

We conclude by pointing out that tunable hyperbolic response in G-hBN devices does not introduce evident losses (Fig. 2b). In fact, the propagation length of HP^3 in G-hBN meta-structures is factor of 1.5–2.0 longer than HP^2 in hBN (Fig. 2). Continuous and reversible tunability of hybrid polaritons in G-hBN meta-structures demonstrated here (Fig. 3) is a significant forte compared with other artificial and natural hyperbolic materials^{12,13,16-18}. Thus, our work uncovers a practical approach for the implementation of nano-photonic meta-structures with intertwined electronic, plasmonic, phonon, and/or exciton polaritonic properties³. Hybridization and tunability effects reported here are expected to be generic for other electromagnetic metamaterials^{31,32} and vdW heterostructures.

Methods

Experimental setup

The infrared (IR) nano-imaging and Fourier transform IR nano-spectroscopy (nano-FTIR) experiments introduced in the main text were performed using a scattering-type scanning near-field optical microscope (s-SNOM). Our s-SNOM is a commercial system (www.neaspec.com) based on a tapping-mode atomic force microscope (AFM). In the experiment, the AFM tip is illuminated by monochromatic quantum cascade lasers

(QCLs) (www.daylightsolutions.com), CO₂ lasers (www.accesslaser.com) and a broad-band laser source via difference frequency generation (DFG) (www.lasnix.com). Together, these lasers cover a frequency range of 700 – 2300 cm⁻¹ in the mid-IR. The s-SNOM nano-images were recorded by pseudo-heterodyne interferometric detection module with an AFM tapping frequency 280 kHz and tapping amplitude around 70 nm. In order to subtract the background information, the s-SNOM output signal was demodulated at the 3rd harmonics of the tapping frequency. In this work, we report our near-field data in the form of the normalized scattering amplitude using gold as the reference: $s(\omega) = s_{\text{sample}}(\omega) / s_{\text{Au}}(\omega)$.

Sample fabrication

Hexagonal boron nitride (hBN) crystals were mechanically exfoliated from bulk samples synthesized as Ref. 33 and deposited onto Si wafers capped with 300 nm thick SiO₂. Graphene was then placed onto the hBN using a PMMA-transfer method. In this work, we use graphene from either mechanical exfoliation or Chemical Vapor Deposition (CVD) synthesis and get the similar results. The CVD synthesis and transfer process were described in Ref. 34. The electrostatic back-gating was accomplished by applying the voltage between the Si wafer and graphene layer.

Acknowledgments:

Work at UCSD is supported by DOE-BES, AFOSR and the Moore foundation. S.-E.Z would like to acknowledge the Young Wild Idea Grant of the Delft Centre for Materials and Delft Energy Initiative Fund. P.J-H acknowledges support from AFOSR grant number FA9550-11-1-0225.

Additional information:

F.K. is one of the cofounders of Neaspec and Lasnix, producer of the s-SNOM and infrared laser used in this work. All other authors declare no competing financial interests.

References:

1. Geim, A. K., & Grigorieva, I. V. Van der Waals heterostructures. *Nature* **499**, 419-425 (2013).
2. Fiori, G. et al. Electronics based on two-dimensional materials. *Nature Nanotech.* **9**, 768-779 (2013).
3. Xia, F., Wang, H., Xiao, D., Dubey, M. & Ramasubramaniam, A. Two-dimensional material nanophotonics. *Nature Photon.* **8**, 899-907 (2014).
4. Britnell, L. et al. Strong Light-Matter Interactions in Heterostructures of Atomically Thin Films. *Science* **340**, 1311-1314 (2013).
5. Novotny, L. & Hecht, B. Principles Of Nano-Optics (Cambridge University Press, Cambridge, 2006).
6. Ju, L. et al. Graphene plasmonics for tunable terahertz metamaterials. *Nature Nanotech.* **6**, 630-634 (2011).
7. Chen, J. et al. Optical nano-imaging of gate-tunable graphene plasmons. *Nature* **487**, 77-81 (2012).
8. Fei, Z. et al. Gate-tuning of graphene plasmons revealed by infrared nano-imaging. *Nature* **487**, 82-85 (2012).

9. Yan, H. et al. Damping pathways of mid-infrared plasmons in graphene nanostructures. *Nature Photon.* **7**, 394-399 (2013).
10. Gerber, J. A., Berweger, S., O'Callahan, B. T. & Raschke, M. B. Phase-Resolved Surface Plasmon Interferometry of Graphene. *Phys. Rev. Lett.* **113**, 055502 (2014).
11. Fang, Z. et al. Active Tunable Absorption Enhancement with Graphene Nanodisk Arrays. *Nano Lett.* **14**, 299-304 (2014).
12. Dai, S. et al. Tunable phonon polaritons in atomically thin van der waals crystal of boron nitride. *Science* **343**, 1125-1129 (2014).
13. Caldwell, J. D. et al. Sub-diffraction, Volume-confined Polaritons in the Natural Hyperbolic Material, Hexagonal Boron Nitride. *Nature Commun.* **5**, 5221 (2014).
14. Xu, X. G. et al. One-dimensional surface phonon polaritons in boron nitride nanotubes. *Nature Commun.* **5**, 4782 (2014).
15. Shi, Z. et al. Amplitude- and phase-resolved nano-spectral imaging of phonon polaritons in hexagonal boron nitride. *Arxiv* (2015). [ArXiv:1501.02343](https://arxiv.org/abs/1501.02343).
16. Jacob, Z. Nanophotonics: Hyperbolic phonon-polaritons. *Nature Mater.* **13**, 1081-1083 (2014).
17. Poddubny, A., Iorsh, I., Belov, P. & Kivshar, Y. Hyperbolic metamaterials. *Nature Photon.* **7**, 948-957 (2013).
18. Guo, Y., Newman, W., Cortes, C. L. & Jacob, Z. Applications of hyperbolic metamaterial substrates. *Advances in OptoElectronics* **2012**, 452502 (2012).

19. Hoffman, A. J. et al. Negative refraction in semiconductor metamaterials. *Nature Mater.* **6**, 946-950 (2007).
20. Jacob, Z., Alekseyev, L. V. & Narimanov, E. Optical Hyperlens: Far-field imaging beyond the diffraction limit. *Opt. Express* **16**, 10455 (2008).
21. Liu, Z., Lee, H., Xiong, Y., Sun, C. & Zhang, X. Far-field optical hyperlens magnifying sub-diffraction-limited objects. *Science* **315**, 1686 (2007).
22. Smith, D. R., Schurig, D., Mock, J. J., Kolinko, P. & Rye, P. Partial focusing of radiation by a slab of indefinite media. *Appl. Phys. Lett.* **84**, 2244-2246 (2004).
23. Hwang, E. H., Sensarma, R. & Das Sarma, S. Plasmon-phonon coupling in graphene. *Phys. Rev. B* **82**, 195406 (2010).
24. Ong, Z. Y. & Fischetti, M. Theory of interfacial plasmon-phonon scattering in supported graphene. *Phys. Rev. B* **86**, 165422 (2012).
25. Brar, V. W. et al. Hybrid Surface-Phonon-Plasmon Polariton Modes in Graphene/Monolayer h-BN Heterostructures. *Nano Lett.* **14**, 3876-3880 (2014).
26. Xu, G. X. et al. Mid-infrared Polaritonic Coupling between Boron Nitride Nanotubes and Graphene. *ACS Nano* **8**(11), 11305-11312 (2014).
27. Cai, W., Shalaev, V. *Optical Metamaterials: Fundamentals and Applications* (Springer, New York, 2010).
28. Woessner, A. et al. Highly confined low-loss plasmons in graphene-boron nitride heterostructures. *Nature Mater.* (2015).

29. Fei, Z. et al. Infrared Nanoscopy of Dirac Plasmons at the Graphene–SiO₂ Interface. *Nano Lett.* **11**, 4701-4705 (2011).
30. Wunsch, B., Stauber, T., Sols, F. & Guinea, F. Dynamical polarization of graphene at finite doping. *New J. Phys.* **8**, 318 (2006).
31. Iorsh, I. V., Mukhin, I. S., Shadrivov, I. V., Belov, P. A. & Kivshar, Y. S. Hyperbolic metamaterials based on multilayer graphene structures. *Phys. Rev. B* **87**, 075416 (2013).
32. Zhang, L. et al. Tunable bulk polaritons of graphene-based hyperbolic metamaterials. *Opt. Express* **22**, 14022 (2014).
33. Watanabe, K., Taniguchi, T. & Kanda, H. Direct-bandgap properties and evidence for ultraviolet lasing of hexagonal boron nitride single crystal. *Nature Mater.* **3**, 404-409 (2004).
34. Li, X. et al. Large-area synthesis of high-quality and uniform graphene films on copper foil. *Science* **324**, 1312-1314 (2009).

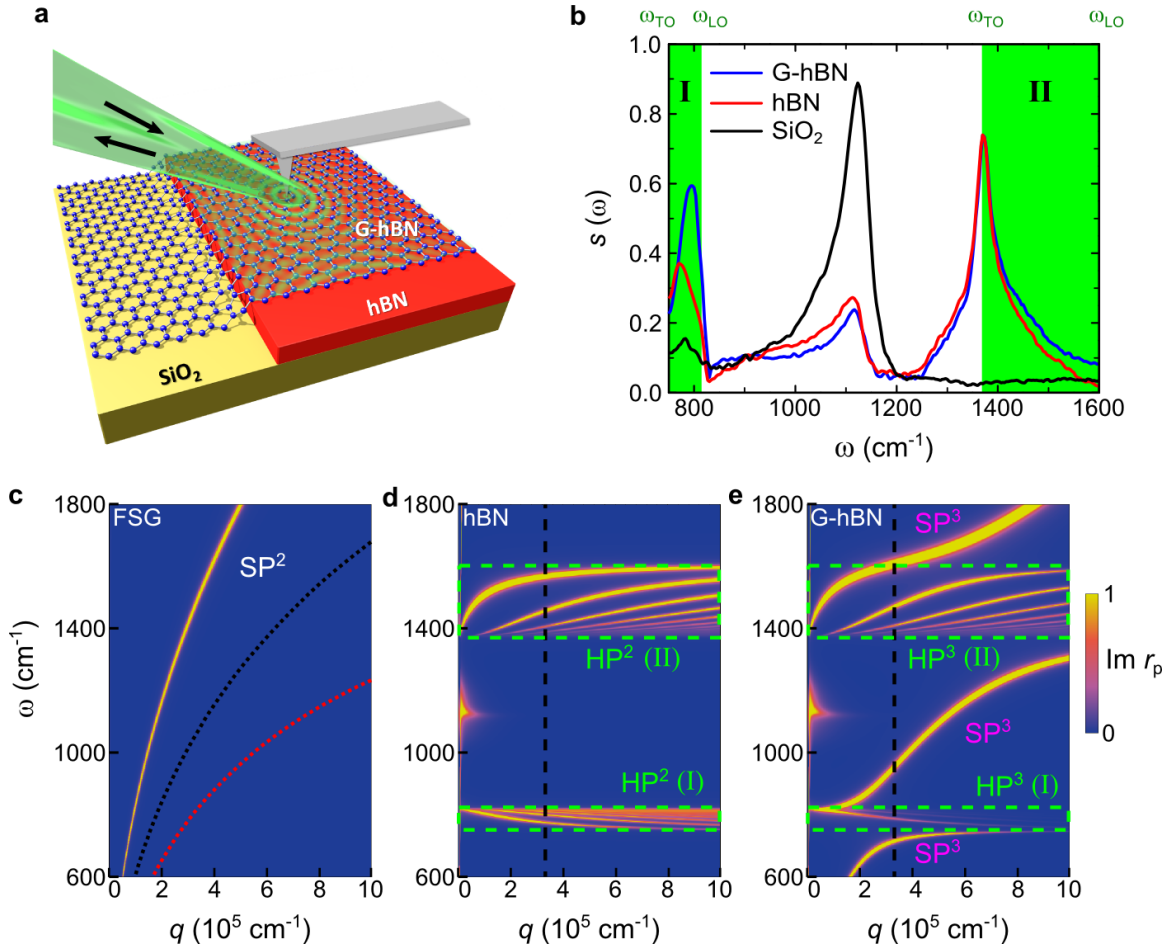


Figure 1 | An Overview of hybridized hyperbolic response in G-hBN meta-structure.

a, The experiment schematic showing the IR beams (the black arrows) incident and back-scattered by an AFM tip. The incident beam is generated from monochromatic or broadband laser sources (Methods). The back-scattered light is collected for extraction of the near-field signal. **b**, Broad-band nano-IR spectra of the meta-structure. The blue, red and black curves represent the spectra for G-hBN, hBN, and SiO₂, respectively. The spectra are collected far away from the sample edges where the impact of edge-reflected polaritonic waves is negligible. **c**, Calculated dispersion of the surface plasmon polariton (SP²) in free-standing graphene (FSG) with Fermi energy $E_F = 0.37, 0.15$, and 0.08 eV. **d**, Calculated dispersion of the hyperbolic phonon polariton (HP²) in hBN of thickness 58

nm. The dispersion is visualized using the false color map of the imaginary part of the reflection coefficient r_p . The black dashed line is a rough estimate of the momentum at which the tip-sample coupling is the strongest²⁹. The green dashed rectangles surround the regions of hyperbolic response. **e**, Same as **(d)** for G-hBN structure with $E_F = 0.37$ eV. The false color map reveals the dispersion of the hyperbolic plasmon-phonon polaritons (HP³) and the surface plasmon-phonon polaritons (SP³).

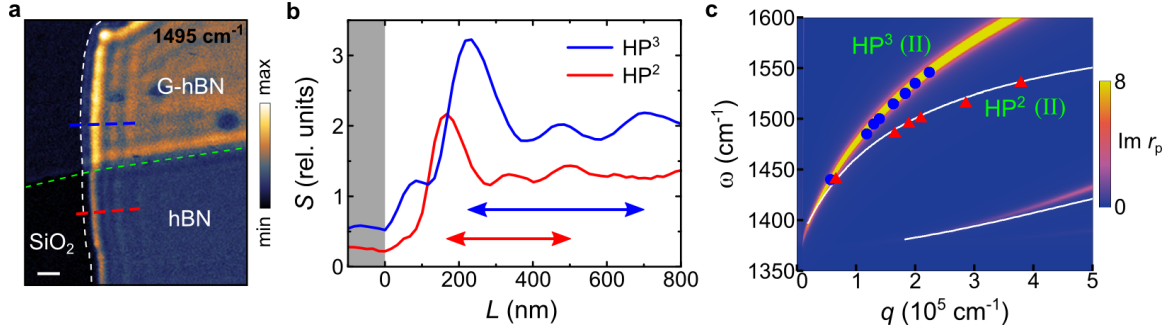


Figure 2 | Modification of type II hyperbolic phonon polaritons in G-hBN meta-structure. **a**, Near-field amplitude image of the G-hBN at frequency $\omega = 1495 \text{ cm}^{-1}$. With a monolayer graphene, the intensity and wavelength of phonon polariton in pristine hBN are increased. White and green dashed lines indicate the edge of hBN and graphene, respectively. Scale bar: 300 nm, $d = 25$ nm. **b**, Line profiles taken along the dashed lines in (a). Double arrows indicate the polariton wavelength measured on G-hBN (blue) and hBN (red). **c**, Experimental dispersion relation of type II HP² in hBN (red triangles) and HP³ in G-hBN (blue dots) with the Fermi energy $E_F = 0.37$ eV. The corresponding simulation results are also provided as the white lines and false color map, respectively.

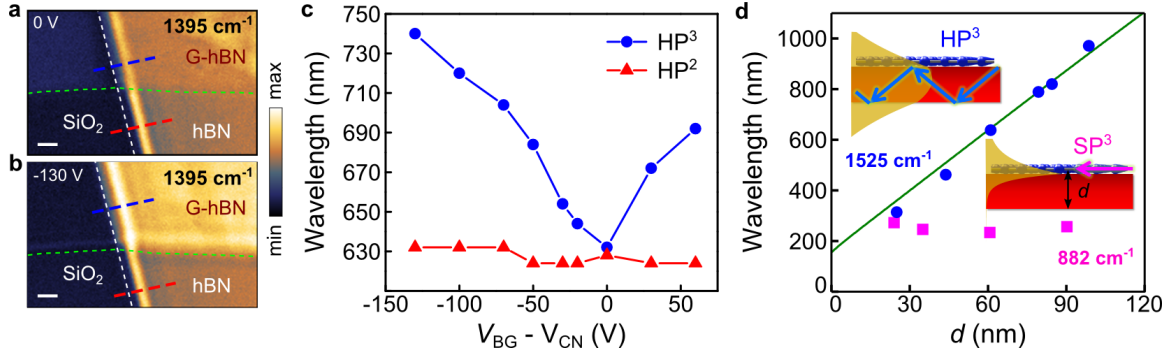


Figure 3 | Tuning of the G-hBN polariton wavelength by electrostatic gating and varying the meta-structure thickness. **a–b**, Near-field images of G-hBN and hBN polaritons at back gate (BG) voltages relative to the charge neutral (CN) state $V_{BG} - V_{CN} = 0$ V (**a**) and -130 V (**b**). Scale bar: 300 nm. **c**, Gate voltage dependence of the HP³ wavelength in G-hBN meta-structure (blue dashed line in Figs. 3a-b) and the apparent lack of thereof for HP² in hBN (red dashed line in Figs. 3a-b) at $\omega = 1395 \text{ cm}^{-1}$. Thickness of the hBN in (**a-c**): $d = 4$ nm. **d**, The dependence of HP³s wavelength on hBN thickness at $\omega = 1525 \text{ cm}^{-1}$ (data and simulations are shown with the blue dots and green line, respectively). For the SP³, there is no systematic thickness-dependence (pink squares). Inset, the propagation schematics for HP³ (top) and SP³ (bottom). Yellow shapes in each inset show the distribution of the real part of the in-plane polariton field.